RSC Advances

ROYAL SOCIETY OF CHEMISTRY

www.rsc.org/advances

Table of Content Entry

Capillarity-Driven (Self-Powered) One-Dimensional Photonic Crystals for Refractometry and (Bio)sensing

By S. Surdo,[a] F. Carpignano,[b] L. Strambini,[a] S. Merlo,[b] and G. Barillaro [a]

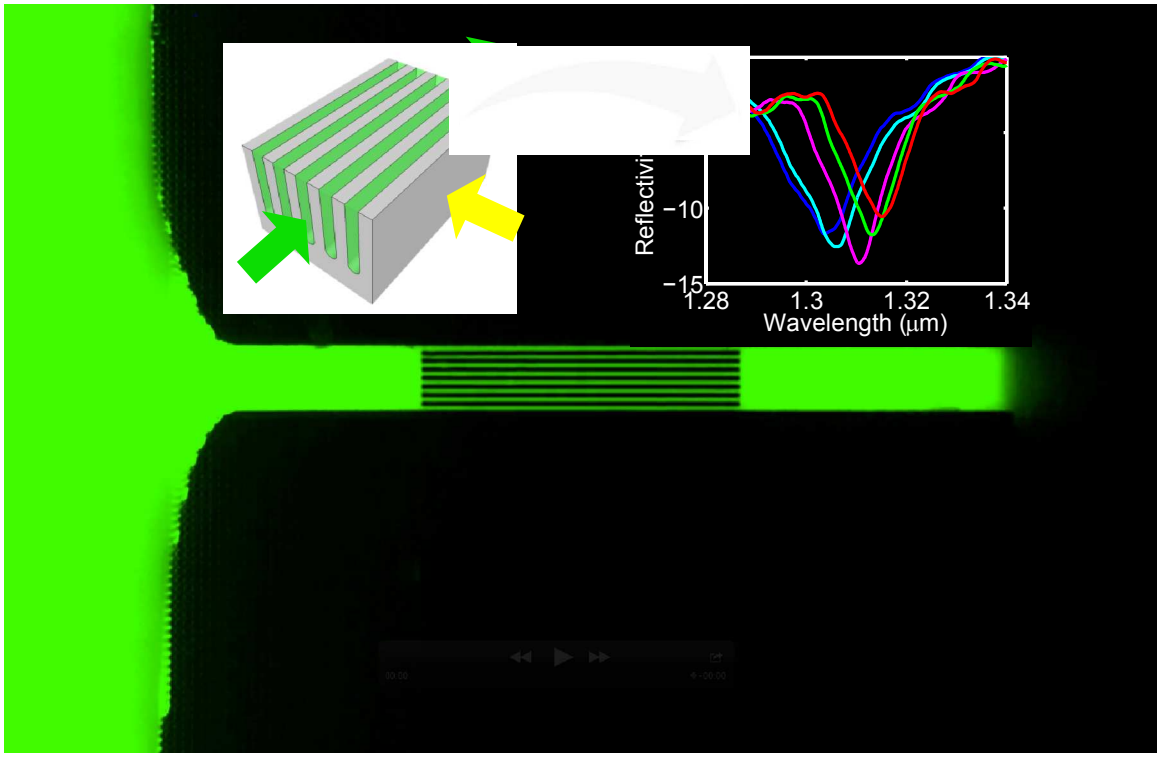

The synergistic use of capillarity and photonic crystals for both refractometry and biosensing applications is demonstrated, both from theoretical and experimental points of view.

Capillarity-Driven (Self-Powered) One-Dimensional Photonic Crystals for Refractometry and (Bio)sensing

S. Surdo,[a] F. Carpignano,[b] L. Strambini,[a] S. Merlo,[b] and G. Barillaro [a*]

[a] Dipartimento di Ingegneria dell'Informazione, Università di Pisa, via G. Caruso 16, 56122 Pisa, Italy; phone: +39 050 2217 601; fax: +39 050 2217 522; email: g.barillaro@iet.unipi.it

[b] Dipartimento di Ingegneria Industriale e dell'Informazione, Università di Pavia, via Ferrata 1, 27100 Pavia, Italy

Abstract

In this work, we advance the state-of-the-art on photonic crystals by demonstrating effective and reliable operation of vertical one-dimensional photonic crystals by capillarity, that is without the use of external pumps, for self-powered label-free refractometry and (bio)sensing applications. As proof-of-concept an all-silicon self-powered drop-and-measure platform exploiting a vertical one-dimensional photonic crystal as sensing element is fabricated and tested by capillary infiltration of both ethanol/water mixtures (used as benchmark for refractometry) and Bovine Serum Albumin (BSA) aqueous solutions at different BSA concentrations (used as benchmark for biosensing). Excellent analytical performance is achieved both for refractometry and biosensing, in terms of reproducibility and linearity, as well as sensitivity and limit-of-detection, thus paving the way towards a novel class of self-powered drop-and-measure platforms for chemical/biochemical point-of-care analysis exploiting photonic crystals operating under capillary operation as label-free transducers.

Introduction

One-dimensional (1D) photonic crystals (PhCs), as well as 2D and 3D PhC structures, have been largely and successfully used for label-free chemical and biochemical sensing [1, and references within it], thanks to their high-sensitivity to tiny changes of both dielectric constant and thickness of the materials composing the PhC structure itself [2-4]. In spite of their high-sensitivity, the delivering of liquids either *over* [2] or *through* [3, 5] the PhC structure has been so far carried out by the use of external pumps (*pressure-driven* operation), which has limited applications of PhCs as sensing elements in self-powered platforms for point-of-care operation.

Capillary microfluidics, which exploits surface tension to handle/move liquids, is a powerful approach enabling the realization of self-powered fluidic platforms for a wide range of applications, from optofluidics, e.g. optical device tuning, to lab-on-chip, e.g. biochemical analysis [6, 7]. Drop-and-measure optofluidic platforms exploit capillary microfluidics to bring the fluid of interest to the optical transducer thus enabling either optical measurement of peculiar fluid parameters, e.g. refractive index, or optical detection of specific biological analytes, e.g C-Reactive Protein (CRP), without any connection to fluidic peripheral equipment [8-12]. The drop-and-measure concept also allows reduction of volume and waste of biological samples, of power dissipation and size of the device, while increasing portability and enabling true point-of-care operation.

In this work, the synergistic use of capillarity and photonic crystals for both refractometry and biosensing applications is successfully demonstrated, both from theoretical and experimental points of view. This allows bridging the gap between pressure-driven photonic crystal structures and capillary-driven sensing platforms by successfully combining high-sensitivity PhCs with self-powering capillary networks, thus advancing the state-of-the-art

literature on both the fields, also with respect to our former work on this subject [3], which mainly addressed pressure-driven operation of vertical 1DPhCs for (bio)sensing.

As a proof-of-concept, a capillary-driven drop-and-measure platform integrating a vertical one-dimensional photonic crystal as label-free sensing elements is both fabricated and tested. Fabrication is performed by deep-etching of silicon through electrochemical micromachining technology. Capillary-flow of liquids over time is investigated through time-resolved measurements and validated through analytical modeling. Optical characterization is carried out by monitoring changes in the reflection spectrum of 1DPhC upon capillary infiltration with ethanol/water mixtures (used as benchmark for refractometry) and Bovine Serum Albumin (BSA) aqueous solutions at different BSA concentrations (used as benchmark for biosensing). Excellent analytical performance of the platform is demonstrated under capillary-action operation, for both refractometry and biosensing applications, in terms of reproducibility and linearity, as well as sensitivity and limit-of-detection.

Design of 1DPhC drop-and-measure platform

Vertical silicon/air 1DPhCs consist of a spatial repetition (in the micrometer scale when operating in the near-infrared region) of high-aspect-ratio silicon walls and air-gaps (Figure 1a). Pressure-driven flow of liquids in the air-gaps (fluidic path) is commonly used to induce a modification of PhC optical properties, which is exploited for label-free either refractometry or (bio)sensing purposes through measurements of reflection or transmission signals perpendicularly to silicon wall surface (optical path). Spontaneous (pump-free) flow of liquids into PhC air-gaps can be also achieved by capillarity once the 1DPhC structure is integrated into a larger microfluidic channel. Each single air-gap of the 1DPhC behaves as an independent rectangular channel with smaller width and, in turn, higher (negative, if referred to atmospheric pressure) capillary pressure with respect to the main microchannel, which enables spontaneous

motion of liquids from the main microchannel to the PhC air-gaps (for wettable silicon surfaces with contact angle <90°).

Figure 1b sketches a self-powered drop-and-measure platform in which an 1DPhC is exploited as label-free sensing element. The 1DPhC is connected to two large reservoirs by two microfluidic channels that are used to effectively infiltrate the 1DPhC air-gaps with liquid by capillary action. Optical path is perpendicular to fluidic path and allow for free-space interrogation of the 1DPhC structure (as well as for positioning/alignment of readout fibers in front of the 1DPhC, if needed [3]). An either glass or polymer slab with inlet/outlet ports is used as cover. The platform makes use of a very simple though functional capillary microfluidic network in which the liquid experiences abrupt changes of the channel cross-section, and, in turn, of the capillary pressure that controls the liquid flow. More specifically, the capillary pressure abruptly decreases from the reservoir (at atmospheric pressure) to the inlet microchannel and to the air-gaps of the 1DPhC, then it snappily increases in the output microchannel and goes back to the atmospheric pressure in the output reservoir [13, 14]. Such a capillary pressure profile allows spontaneous infiltration of the liquid dropped in the reservoir to the inlet microchannel, the PhC structure, and then to the outlet microchannel. Eventually, the liquid stops at the end of the output microchannel, which works as a capillary retention-valve thanks to its 90-degrees end-corners [15], thus allowing liquid retention in the PhC air-gaps for times long enough to perform incubation of biomolecules in the PhC as well as to carry out optical measurements of PhC reflection/transmission properties upon infiltration.

The platform is designed to be symmetric with respect to the 1DPhC structure, and, therefore, it can operate under capillarity in both directions, that is left-to-right and right-to-left.

Fabrication and characterization of 1DPhC drop-and-measure platform

Two 1DPhC drop-and-measure platforms of the type reported in Figure 1b are simultaneously integrated on the same chip. The two platforms feature an 1DPhC with same spatial period 8 μm, air-gap width 5 μm, length 300 μm, and height 90 μm, but with different number of air-gaps *n*, namely 8 and 12. The 1DPhC is connected to two large reservoirs (2000 μm × 2000 μm) by two microfluidic channels with same length 250 μm, height 90 μm, and width *w,* namely 61 and 101 μm for the two platforms. Optical path has width 300 μm and height 90 μm for both the platforms.

Fabrication of the platforms is carried out by electrochemical micromachining (ECM) technology [16], according to the technological process detailed in Ref. [3]. The starting material is *n*-type silicon, orientation (100), with a thin (100-nm-thick) silicon dioxide layer on top. The layout of the platform to be fabricated is patterned on a photoresist layer by standard lithography, transferred to the silicon dioxide layer by buffered HF (BHF) etching through the photoresist mask, replicated into the silicon surface by potassium hydroxide (KOH) etching through the oxide mask, and finally grooved into the silicon bulk by back-side illumination electrochemical etching (BIEE) in aqueous electrolytes containing traces (5% by vol.) of HF. A sketch of the main technological steps of the fabrication process is reported in Figure S1 (Supplementary Information). Figure 2 shows scanning electron microscope (SEM) pictures a 1DPhC drop-and-measure platform with n=12, at different magnifications. In Figure 2a a top-view of the whole platform is shown, in which it is possible to discriminate the 1DPhC integrated in the middle of optical and fluidic paths. Figures 2b (top-view) and 2c (bird-eye-view) show magnifications of the 1DPhC, in which it is possible to appreciate the high accuracy in microfabrication and high quality of silicon surfaces.

After fabrication, the platform is subjected to Piranha treatment (H_2SO_4 (95-98%):H_2O_2 (30%)=3:1 by vol. for 15 minutes at room temperature) in order to modify the chemistry of silicon surfaces from Si-H to Si-OH, thus switching from hydrophobic to hydrophilic surfaces

[17]. Effectiveness of Piranha treatment is verified by measuring the contact angles of flat silicon surfaces after both HF and Piranha treatments, by standard static sessile drop method, which yields contact angles of 58.4°±4.3° and 3.2°±0.3°, respectively.

Mixtures of water and ethanol at different concentrations (ethanol from 0% to 80% (by vol.) with step 20%) containing 0.15 mg/ml of fluorescein are used to investigate capillary flow of liquids in the platform, through the use of a fluorescence microscope equipped with a high-speed (36 fps) camera. For all the tested mixtures a calibrated volume of 0.4 μl of liquid is dropped into one of the reservoirs. The liquid quickly infiltrates the first microchannel (about 1s for water) connecting the reservoir with the 1DPhC, then the 1DPhC (about 0.2 s for water) and the second microchannel (about 3 s for water). Eventually, the liquid stops at the end of the second microchannel, thus retaining the liquid in the 1DPhC structure for optical measurements (>30 min for water). An average time of 4.2 s is required to fully infiltrate the platform with water. A typical time-resolved sequence of fluorescence microscope images showing capillary flow of water in the platform is reported in Figure 3. Capillary pressure, speed, and position of the liquid/air meniscus along both the main microchannel and the PhC integrated within it can be analytically calculated starting from basic equations on capillarity [13-15], once geometrical dimension of the channel, chemistry termination of silicon surfaces, and liquid to be injected are defined. Experimental capillary infiltration dynamics of the platform well agrees with theoretical capillary infiltration dynamics once dimension, surface roughness, and surface termination of both the microchannels connecting 1DPhC to the reservoirs and the PhC structure itself are taken into account, as shown in Figure S2 (Supplementary Information). Details on the theoretical modeling of the platform are given in Supplementary Information.

Optical characterization of the drop-and-measure platform is carried out by measuring reflection spectra of the 1DPhC structure upon capillary infiltration with the different liquid solutions. Specifically, ethanol/water mixtures with different concentration of ethanol are used as

benchmark for refractometry applications; Bovine Serum albumin (BSA) solutions in water at different BSA concentrations are used as benchmark for (bio)sensing applications.

A bidirectional 2x2 single mode fiberoptic coupler with 50:50 coupling ratio is used to carry broadband radiation toward the 1DPhC and to redirect the back reflected light toward the monochromator input of an optical spectrum analyser. A pigtail style focuser with aspheric lens connected at the output port of the coupler is used as readout termination to generate a low divergence beam yielding a 50-μm diameter spot (area under investigation) on the 1DPhC at the working distance of about 23.5 mm. All the employed fiber components use standard telecommunication optical fibers (9/125 core/cladding diameter) with FC connectors. The unused output port of the coupler is terminated with an APC/FC connector to avoid spurious back reflections. The drop-and-measure platform is placed on a x-y-z precision micropositioner, whereas the readout lens is secured on a kinematic mount for optics. A white light source (WLS, Tungsten lamp) with approximately constant power density in the wavelength range 1.0-1.7 μm is preliminary used to measure the reflection spectrum of the 1DPhC in water over a large wavelength interval (resolution bandwidth RB=10 nm). A superluminescent diode (SLED) with Gaussian emission spectrum centred at about 1.3 μm (full width half maximum FWHM=75 nm), for which the fabricated 1DPhC structure filled with water-based solutions features a reflectivity notch, is used to finely investigate (RB=70 pm) the reflection properties of the 1DPhC upon capillary infiltration with the different liquid mixtures. A schematic of the fiber-optic setup used for carrying out the reflectivity measurements on the drop-and-measure platform is shown in Figure S3 (Supplementary Information).

For all the tested mixtures, a calibrated volume of 0.4 μl of liquid is dropped into one of the reservoir, then the liquid readily infiltrates the 1DPhC structure and the reflectivity spectrum of the 1DPhC is acquired at several sampling times. For each mixture the procedure is repeated

several times, so as to infer on both single-drop and drop-to-drop reproducibility of the measurements.

Benchmark tests for refractometry applications are carried out using ethanol/water mixtures with ethanol concentrations ranging from 0% to 80% with step 20%. Figure 4a shows typical reflectivity spectra, upon SLED excitation, of the 1DPhC of the platform after capillary infiltration with the different ethanol/water mixtures. A red shift of the notch wavelength position is apparent, which can be explained in terms of increased refractive indices of the mixtures as the ethanol concentration increases. Figure 4b reports the calibration curve of the platform for ethanol/water mixtures, that is the notch wavelength position (mean value and standard deviation) versus the refractive index of the mixtures infiltrated in the PhC structure. Each point represents the notch wavelength of a Lorentzian fit of experimental reflectivity spectra. The refractive index values of the different water/ethanol mixtures are estimated by using the Lorentz-Lorentz law [18]. Analytical performance of the platform is evaluated in terms of reproducibility, linearity, sensitivity, and resolution. Reproducibility is evaluated in terms of coefficient of variation $\%CV=\sigma/\mu*100$, with σ standard deviation and μ mean value of experimental data. Linearity is evaluated in terms of squared correlation coefficient R^2 of the linear regression curve best-fitting experimental data. Sensitivity S is evaluated in terms of slope of the linear regression curves best-fitting experimental data. Resolution is evaluated in terms of limit of detection $LoD=3\sigma/S$, with σ standard deviation value of the experimental notch position in water, which is used as reference solution. Excellent reproducibility ($\%CV<0.02\%$) and linearity ($R^2>0.98$), as well as high sensitivity (S=430 nm/RIU) and good limit-of-detection ($LoD=1.4\times10^{-5}$ RIU) are achieved. Analytical performance of the platform is either comparable to (e.g., capillary ring resonators) or better than (e.g., 2-D PhCs, planar ring resonators, microsphere ring resonators) integrated state-of-the-art refractometers under pressure-driven operation [19].

Benchmark tests for label-free biosensing applications are carried out using BSA aqueous solutions at different concentrations in the range 0.1%-7%. An average incubation time of 5 minutes is used for all BSA solutions, which is compatible with evaporation of solution from the 1DPhC structure. Figure 4c show typical reflectivity spectra of the 1DPhC of the platform upon capillary infiltration with the different BSA solutions. A red shift of the notch wavelength position is evident as the BSA concentration increases, which can be explained in terms of both modification of the PhC structure by BSA adsorption on the *xz* plane of PhC silicon walls (surface effect) and increased refractive index of the mixtures flowing in the PhC air-gaps (volume effect). Figure 4d reports the calibration curve of the platform for BSA solutions, that is notch wavelength position (mean value and standard deviation) versus both BSA concentration (top x-axis) and refractive index (bottom x-axis) of BSA/water mixtures [20] infiltrated into the 1DPhC structure. Each point represents the notch wavelength of a Lorentzian fit of experimental reflectivity spectra. Two different linear regimes are evident in Figure 4d as the BSA concentration increases from 0.1% to 7%. A higher-sensitivity regime (either S=3000 nm/RIU or S=5.5 nm/%) occurs for lower BSA concentrations (below 1%); a lower-sensitivity regime (either S=490 nm/RIU or S=0.9 nm/%) occurs for higher BSA concentrations (above 1%). These two regimes can be explained in terms of surface and bulk effects due to non-specific adsorption of BSA on the PhC silicon surfaces (*xz* plane) and refractive index variation of BSA solutions flowing in the PhC air-gaps, respectively. It is well know that surface coverage is dependent on the BSA concentration in solution and can be modeled by the Langmuir equation [21]. At the lower BSA concentrations, both surface and volume effects influence PhC reflection properties. Nonetheless, the formation of an adsorbed BSA layer on the silicon surfaces, with a surface coverage increasing with BSA concentration of solutions flowing in the PhC air-gaps, produces structural changes on the 1DPhC that dominate PhC reflection properties at the lower BSA concentrations. At the higher BSA concentrations, surface coverage due to BSA adsorption on

the silicon surfaces tends to saturate, so that variation of the refractive index of BSA solutions flowing in the PhC air-gaps dominates PhC reflection properties [22-24]. Note that at higher BSA concentrations the sensitivity value is 490 nm/RIU, as calculated through best-fitting of experimental data, which is consistent with the sensitivity value obtained for ethanol/water mixtures (430 nm/RIU) and explainable in terms of volume effects due to refractive index variations. By assuming volume effects to be constant over the whole range of investigated BSA concentrations, surface sensitivity due to only BSA adsorption on PhC silicon surfaces can be achieved by depurating the sensitivity values at the lower BSA concentrations from volume effects, thus obtaining S=2510 nm/RIU (S=4.6 nm/%). Excellent reproducibility (%CV<0.05%) and linearity (R^2>0.98), as well as good limit-of-detection (LoD either $2x10^{-6}$ RIU or 0.001%) are achieved, which is either comparable or better than most of state-of-the-art pressure-driven biosensors.

Modeling of capillary infiltration of 1DPhC drop-and-measure platform

The fluidic path of the drop-and-measure platform tested in this work consists of a series of three components: 1) a inlet microchannel Ch1 (width w_1=61 μm, height h_1=90 μm, length l_1=250 μm) connecting the inlet reservoir to the 1DPhC; 2) an 1DPhC, consisting from a fluidic point of view of n independent microchannels (width w_2=5 μm, height h_2=90 μm, length l_2=300 μm, n = 8); 3) an output microchannel Ch2 (width w_3=61 μm, height h_3=90 μm, length l_3=250 μm) connecting the 1DPhC to the outlet reservoir. All these fluidic components are simultaneously fabricated in a silicon substrate by ECM technology, then the platform is provided with either glass or polymeric cover on top. Both the microfabricated silicon substrate and cover are treated in Piranha solutions so as to have same OH termination of surfaces and, in turn, same contact angle θ. It must be noted that, ECM makes use of both functional and sacrificial structures for the fabrication of complex microsystems, which are functional to the

microsystem operation and sacrificed for the microsystem fabrication. In the specific case of the platform of this work sacrificial structures are used for the fabrication of optical and fluidic paths, which after removal gives rise to an artificial periodic ripple (peak-to-peak amplitude about 100 nm) at the bottom and side surfaces of both fluidic and optical paths. Such an artificial ripple, which can be clearly seen in Figure S2, works as surface roughness in fluidic paths, thus increasing fluidic losses of channel Ch1 and Ch2 with respect to 1DPhC, which is fabricated without the use of sacrificial structures and has surface roughness as low as 10 nm [3, 16]. Such a difference in surface finishing between fluidic channels Ch1 and Ch2 and the 1DPhC cannot be neglected and is taken into account for the correct fluidic modeling of the platform of this work. More in detail, a non-dimensional coefficient μ is introduced to capillary equations to take into account different viscous losses of fluidic channels Ch1 and Ch2 due to the different roughness of surfaces, as described here in the following.

For capillary flow of the liquid within the inlet microchannel Ch1 ($0<x<l_1$), which is opened at both ends, capillary pressure P_{c1} at the liquid/air meniscus can be expressed as:

$$P_{c1}(x) = -\gamma \cos\theta \frac{p_1}{S_1} \qquad (1)$$

where x is the position along the channel, θ is the contact angle at the liquid/solid interface which are supposed to be roughness-free, γ is the surface tension of the liquid, $p_1=2(w_1+h_1)$ and $S=w_1h_1$ are perimeter and section area of Ch1, respectively. For contact angles $0°\leq\theta<90°$, the pressure drop ΔP across the liquid in the microchannel is $\Delta P=|P_{c1}|>0$, which highlights that the capillary pressure is responsible for capillary motion of liquid within the microchannel.

Mean speed v_{c1} of the liquid/air meniscus within the inlet microchannel Ch1 can be expressed, under assumption of laminar flow, as:

$$v_{c1}(x) = \left(\frac{C_1}{\eta}\right)\frac{|P_{c1}|}{x} \qquad (2)$$

where η is the dynamic viscosity of the liquid, and $C_1=S_1^2/2\mu_1 p_1^2$ is a constant value, also known as dissipation factor, where μ_1 is the non-dimensional coefficient introduced to take into account increased viscous losses due to surface roughness in Ch1.

Time needed by the liquid/air meniscus to travel along the microchannel is obtained through integration of Eq. 2:

$$t_{c1}(x)=\frac{\eta}{2C_1|P_{c1}|}x^2 \qquad (3)$$

As for capillary flow in the 1DPhC and in the output microchannel Ch2, on the one hand, Eq. 1 also describes capillary pressure in each single air gap of the 1DPhC ($l_1<x<l_1+l_2$), as well as in the output microchannel Ch2 ($l_1+l_2<x<l_1+l_2+l_3$), once the suitable values for p and S are used. On the other hand, application of the equation of continuity for the liquid mass flow rate in the net of channels of the platform, namely between Ch1, air-gaps of 1DPhC and Ch2, allows mean speed v_{c2} and v_{c3}, and in turn filling time, within the 1DPhC and the output channel Ch2 to be calculated from Eq. 2, obtaining for the 1DPhC and for Ch2, respectively:

$$v_{c2}(x)=\left(\frac{C_2}{\eta}\right)\frac{|P_{c2}|}{(x-l_1)+(l_1 n)\left(w_2C_2/w_1C_1\right)} \qquad (4)$$

$$v_{c3}(x)=\left(\frac{C_3}{\eta}\right)\frac{|P_{c3}|}{(x-l_2)+\left(l_2/n\right)\left(w_3C_3/w_2C_2\right)} \qquad (5)$$

where, $C_2=S_2^2/2\mu_2 p_2^2$ and $C_3=S_3^2/2\mu_3 p_3^2$ are the dissipation factors and μ_2 and is μ_3 are the non-dimensional coefficient taking into account viscous losses due to surface roughness within the 1DPhC and Ch2, respectively.

By properly integrating v_{c2} and v_{c3} it is feasible to get time position t_{c2} and t_{c3} of the liquid/air meniscus within the 1DPhC ($l_1<x<l_1+l_2$) and Ch2 ($l_1+l_2<x<l_1+l_2+l_3$), respectively:

$$t_{c2}(x)=t_1+\frac{\eta}{2C_2|P_{c2}|}\left(x^2+\alpha_2 x-\beta_2\right) \qquad (6)$$

$$t_{c3}(x) = t_2 + \frac{\eta}{2C_3|P_{c3}|}\left(x^2 + \alpha_3 x - \beta_3\right) \quad (7)$$

where $t_1=t_{c1}(l_1)$, $\alpha_2 = 2l_1\left(n w_2 C_2 / w_1 C_1\right) - 2l_1$, $\beta_2 = l_1\left(\alpha_2 + l_1\right)$, and $t_2=t_{c2}(l_1+l_2)$, $\alpha_3 = 2l_2\left(w_3 C_3 / n w_2 C_2\right) - 2l_2$, $\beta_3 = \left(l_1 + l_2\right)\left(\alpha_3 + l_1 + l_2\right)$.

By assuming that water is infiltrating the platform (η=1×10^{-3} Pa·s, γ=73×10^{-3} N/m^2, contact angle θ=3.2°) experimental time-resolved data are best-fitted with $\mu_1=\mu_3$=20.8×10^3 and μ_2=12.

Figure 5 shows theoretical capillary pressure P_c, mean speed $v_c(x)$ and time position $t_c(x)$ of the liquid/air meniscus along the fluidic path of the drop-and-measure platform calculated for the case of water, which are in good agreement to experimental results on the platform infiltration kinetics.

Conclusions

In this work vertical, effective and reliable operation of vertical one-dimensional photonic crystals by capillarity, that is without the use of external pumps, for self-powered label-free refractometry and (bio)sensing applications is demonstrated by fabrication and testing of an autonomous drop-and-measure platform. The integrated platform is benchmarked for both reractometry and (bio)sensing applications, showing high sensitivity and good limit of detection, as well as excellent reproducibility and linearity, which are comparable to best stand-alone state-of-the art pressure-driven devices. Breakthrough in point-of-care applications is envisaged by building on the synergistic use of photonic crystals and capillarity.

Acknowledgements

This research was partially funded by the Fondazione CARIPLO, Grant No. 2011-0308, and by the Italian Minister for University and Research (MIUR) Futuro in Ricerca (FIR)

programme, Grant No. RBFR122KL1 (SENS4BIO). The authors wish to thank Dr. G. Mazzini for providing BSA solutions and for fruitful discussions.

References

1 Y. Zhao, X. Zhao and Z. Gu, *Adv. Funct. Mater.*, 2010, **20**, 2970;

2 S. Mandal, J. M. Goddard and D. Erickson, *Lab Chip*, 2009, **9**, 2924;

3 S. Surdo, S. Merlo, F. Carpignano, L.M. Strambini, C. Trono, A. Giannetti, F. Baldini and G. Barillaro*, Lab Chip*, 2012, **12**, 4403;

4 W. Shen, M. Li, B. Wang, J. Liu, Z. Li, L. Jiang, Y. Song, *Journal of Materials Chemistry* 2012, 22, 8127;

5 Y. Guo, H. Li, K. Reddy, H. S.Shelar, V. R. Nittoor, X. Fan, *Applied Physics Letters*, 2011, **98**, 041104;

6 S. Haeberle and Z. R. Zengerle, *Lab Chip*, 2007, **7**, 1081;

7 L. Gervais, N. de Rooij and E. Delamarche, *Adv. Mater.*, 2011, **23**, H151;

8 E. Delamarche, A. Bernard, H. Schmid, B. Michel and H. Biebuyck, *Science*, 1997, **276**, 779;

9 R. Safavieh and David Juncker, *Lab Chip*, 2013, **13**, 4180;

10 G. Zhou, X. Mao and D. Juncker, *Anal. Chem.*, 2012, **84**, 7736;

11 L. Gervais, M. Hitzbleck and E. Delamarche, *Biosens. Bioelectron.*, 2011, **27**, 64;

12 D. Juncker, H. Schmid, U. Drechsler, H. Wolf, M. Wolf, B. Michel, N. de Rooij and E. Delamarche, *Anal. Chem.*, 2002, **74**, 6139;

13 L-J. Yang, T-J. Yao and Y-C. Tai, *J. Micromech. Microeng.*, 2004, **14**, 220;

14 M. Zimmermann, H. Schmid, P. Hunziker and E. Delamarche, *Lab Chip*, 2007, **7**, 119;

15 M. Zimmermann, P. Hunziker and E. Delamarche, *Microfluid Nanofluid*, 2008, **5**, 395;

16 M. Bassu, S. Surdo, L. M. Strambini, *Adv. Funct. Mater.*, 2012, **22**, 1222.

17 X. Li, Y. He, M. T. Swihart, *Langmuir* 2004**, 20***,* 4720;

18 J. V. Herráez and R. Belda, *J. Solution Chem.*, 2006, **35**, 1315;

19 I. M. White and X. Fan, *Opt. Express*, 2008, **16**, 1021;

20 T. Tumolo, L. Angnes and M. S. Baptista, *Anal. Biochem.*, 2004, **333**, 273;

21 H.-J. Butt, K. Graf, and M. Kappl, 2003 Physic and Chemistry of Interfaces, WILEY-VCH, Weinheim.

22 D. Dorfner, T. Zabel, T. Hurlimann, N. Hauke, L. Frandsen, U. Rant, G. Abstreiter, and J. Finley, *Biosens. Bioelectron*., 2009, **24**, 3688.

23 S. Kita, S. Hachuda, S. Otsuka, T. Endo, Y. Imai, Y. Nishijima, H. Misawa, and T. Baba, *Opt. Express*, 2011,**19**, 17683.

24 M. I. Lapsley, I.-K. Chiang, Y. B. Zheng, X. Ding, X. Mao, and T. J. Huang, *Lab Chip*, 2011, 11, 1795.

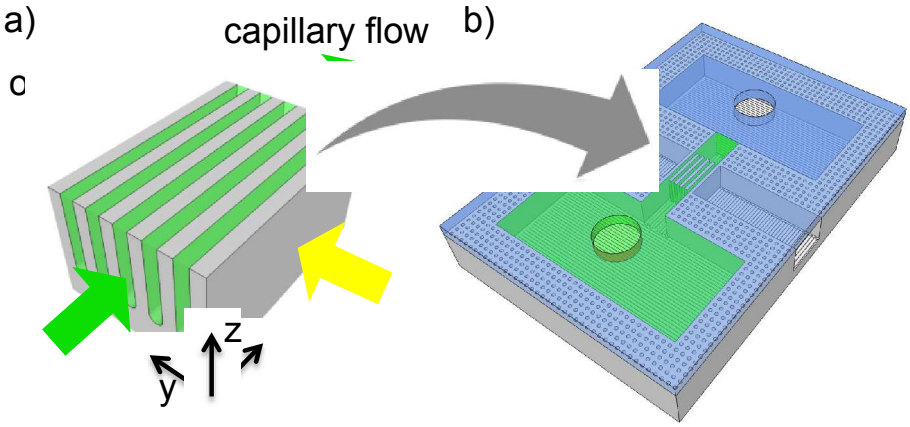

Figure 1. 1DPhC self-powered drop-and-measure platform. (a) Schematic representation of a vertical silicon/air 1DPhC in which fluidic path through the air gaps and optical path perpendicular to silicon walls are highlighted. (b) Drop-and-measure platform exploiting an 1DPhC operating under capillary-action as label-free sensing element.

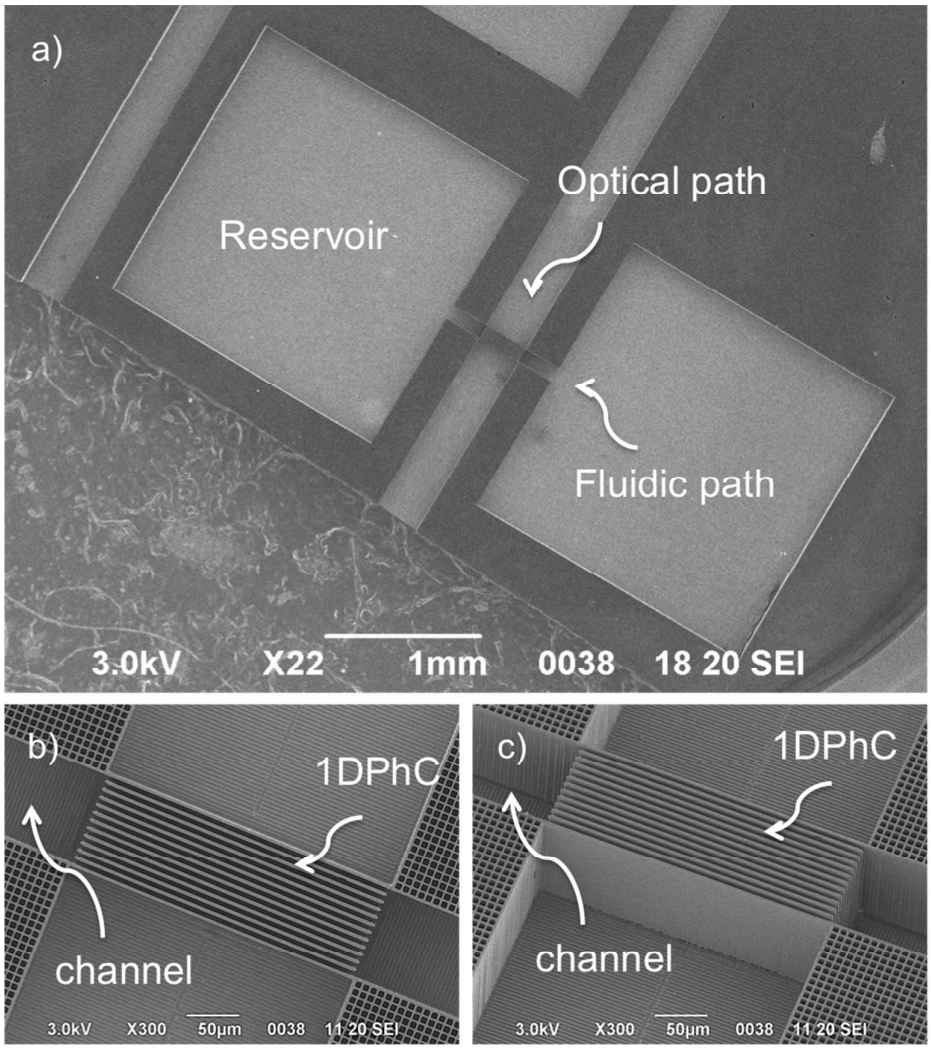

Figure 2. SEM images of the 1DPhC self-powered drop-and-measure platform. (a) Top-view of the whole platform showing the 1DPhC, which is exploited as label-free sensing element operating under capillary-action, in the middle between optical and fluidic paths. (b, c) Top-view (b) and bird-eye-view (c) magnifications of the 1DPhC structure.

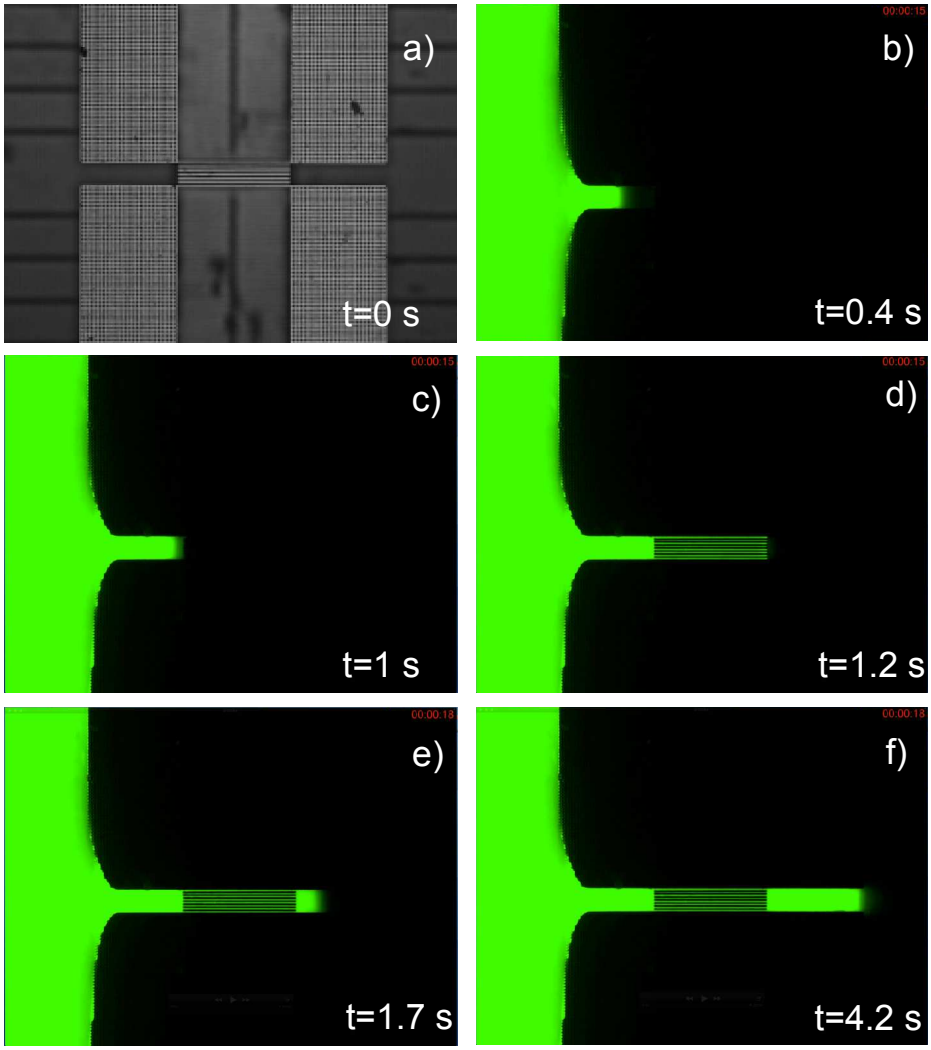

Figure 3. Time-resolved capillary infiltration of the 1DPhC self-powered drop-and-measure platform. (a) Bright-field microscope image and (b-f) fluorescence microscope images, respectively, before and after dropping 0.4 µl of water containing 0.15 mg/ml of fluorescein in the left-hand-side reservoir, respectively, at different times. Images (b-f) clearly highlight capillary flow of water within the platform: infiltration of the microchannel on the left (b, c); infiltration of the 1DPhC structure (d); infiltration and stop of the microchannel on the right (e, f).

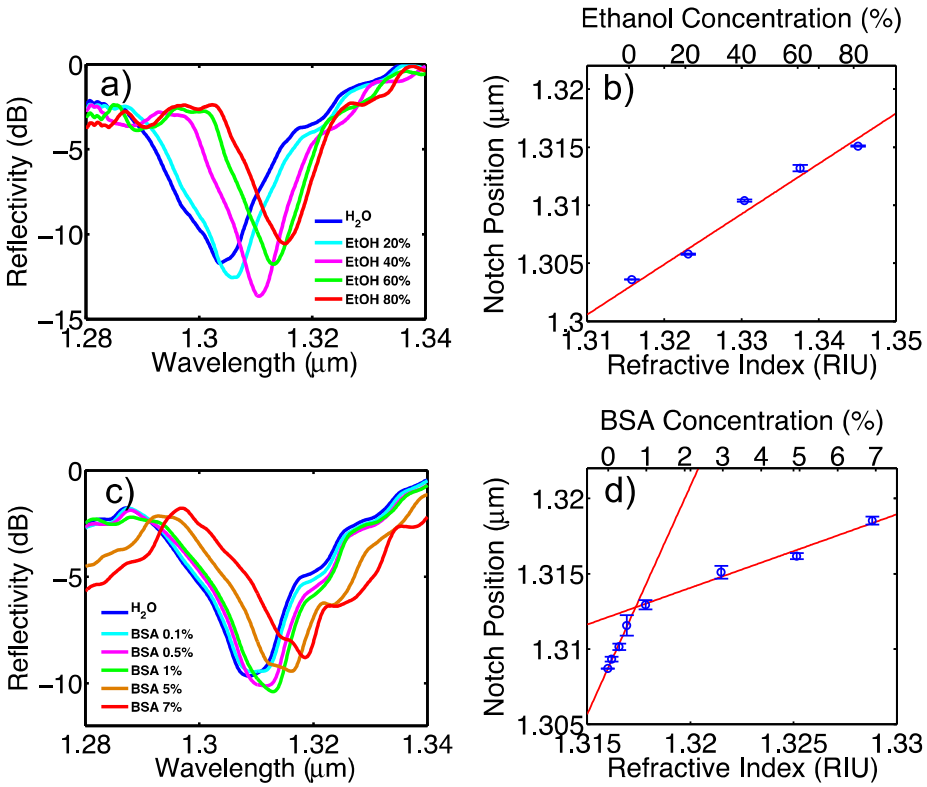

Figure 4. Optical characterization of the 1DPhC self-powered drop-and-measure platform. (a, c) Typical reflectivity spectra (around 1.3 μm) of the 1DPhC upon capillary infiltration with ethanol/water mixtures (a) and BSA solutions (c). (b, d) Calibration curves of the 1DPhC upon capillary infiltration with ethanol/water mixtures (b) and BSA solutions (d).

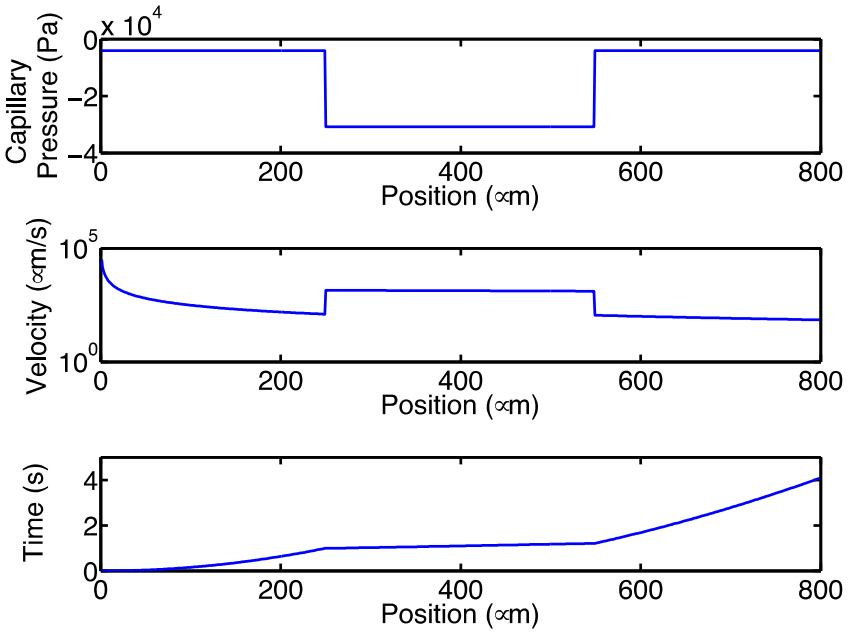

Figure 5. Theoretical capillary pressure P_c, mean speed $v_c(x)$ and time position t_c of the liquid/air meniscus along the fluidic path of the self-powered drop-and-measure platform of this work calculated for the case of water.